19th Australasian Fluid Mechanics Conference
Melbourne, Australia
8-11 December 2014

# Hydrodynamic Stability Analysis on Inviscid Cross Sheared Stratified Flows

**Y. Xiao[1], W. Lin[1,2], S. W. Armfield[3], M. P. Kirkpatrick[3] and Y. He[1]**

[1]College of Science, Technology & Engineering
James Cook University, Townsville, QLD 4811, Australia

[2]Solar Energy Research Institute,
Yunnan Normal University, Kunming, Yunnan 650092, China

[2]School of Aerospace, Mechanical and Mechatronic Engineering
The University of Sydney, NSW 2006, Australia

## Abstract

In this study, linear perturbation equations for CSS flows, in which two comparable orthogonal basic flow velocities (streamwise and spanwise velocities) coexist in a stratified environment, are derived in terms of a characteristic parameter, the cross shear ratio $\xi = \Delta v_0/\Delta u_0$, where $\Delta u_0$ and $\Delta v_0$ are the initial streamwise and spanwise velocity changes across the sheared layer, respectively. The stability features of a cross free sheared flow, a cross bounded sheared flow, and a cross jet flow with specific velocity and stratification profiles are obtained. The results show that the unstable regions of all these three types of CSS flows stretch towards large values of the local Richardson number $Ri_g$ with the introduction of the spanwise velocity, and the growth rate of the perturbation increases significantly when $\xi$ increases. As a result of such a stretching effect, the stability boundary in terms of the critical local Richardson number $Ri_{g,cr}$ expands with increasing $\xi$ and exceeds $Ri_{g,cr} = 0.25$, a value predicted by the classic Miles-Howard theorem.

## Introduction

Hydrodynamic analysis, which studies the critical conditions and the effective domain for flow instability, plays an important role in the study of sheared stratified (SS) flows. So far, the majority of the hydrodynamic analysis on SS flows has been prompted by the earlier linear stability analysis on parallel sheared stratified (PSS) flows, where the basic flow velocity components satisfy $V \ll U$, where $U$ and $V$ are the streamwise and spanwise components of the basic flow in the $x$ and $y$ directions, respectively. The linear stability analysis was initiated by the studies on PSS flows by deriving the Taylor-Goldstein (TG) equation, and the classical Miles-Howard theorem predicts that $Ri_g \leq 0.25$, where $Ri_g$ is the local Richardson number, is the critical condition for a stationary unstable mode under infinitesimal perturbations. Such an unstable mode corresponds to the Kelvin-Helmholtz (KH) instability. By considering the ratio between the sheared layer thickness and the stratified layer thickness, Hazel [1] solved the TG equation numerically and obtained the Holmboe instability.

In contrast to a 'parallel' flow with $V \ll U$, a SS flow with comparable $V$ and $U$ can be appropriately named a 'cross' sheared stratified (CSS) flow. The past studies on CSS flows, although very scarce, revealed distinctive and more complicated flow instabilities. For example, Atsavapranee & Gharib [2] observed experimentally smaller spanwise eddy structures developed from the 'braid' region of the main streamwise KH eddy, whereas Lin *et al.* [3] examined numerically the effects of the cross shear stresses on a two-layer stratified flow. A common and noteworthy conclusion from both these studies is that the mixing effect of CSS flows is significantly enhanced compared to PSS flows at the same conditions.

Although CSS flows seem to be a promising basic flow configuration in terms of the mixing effect, to our best knowledge, the relevant stability analysis has not been reported, which motivates this study. Based on the previous studies on CSS flows and the stability analysis on PSS flows by Hazel [1], this study derives the linearized perturbation equations for CSS flows by adding the spanwise basic velocity $V$ in the original Taylor-Goldstein equation system. The introduction of $V$ brings in a new, and unique, characteristic parameter called the cross shear ratio, $\xi = \Delta v_0/\Delta u_0$, for CSS flows, where $\Delta u_0$ and $\Delta v_0$ are the initial streamwise and spanwise velocity changes across the sheared layer in the $x$ and $y$ directions, respectively. With $\xi$, the two-dimensional TG equation can be extended to three-dimensional complex basic flow states so that a PSS flow becomes a special case of a CSS flow with $\xi = 0$. Using the derived perturbation equations for CSS flows, this study then examines the linear stability features of three CSS flows, *i.e.*, a cross free sheared flow, a cross bounded shear flow, and a cross jet flow. The PSS flow counterparts of each of the three CSS flows are also examined as the $\xi = 0$ case.

## Linearized Perturbation Equations

With the Boussinesq approximation, the governing equations for an inviscid, incompressible, stratified flow are,

$$\nabla_* \cdot \mathbf{u}_* = \mathbf{0} \tag{1}$$

$$\bar{\rho}_* \frac{\partial \mathbf{u}_*}{\partial t_*} + \bar{\rho}_* (\mathbf{u}_* \cdot \nabla_* \mathbf{u}_*) = -\nabla_* p_* - g(\rho_* - \bar{\rho}_*)\vec{k} \tag{2}$$

$$\frac{\partial \rho_*}{\partial t_*} + \mathbf{u}_* \cdot \nabla_* \rho_* = 0 \tag{3}$$

in which $\mathbf{u}_*$ is the velocity vector with the components ($u_*$, $v_*$, $w_*$) in the Cartesian coordinates ($x_*$, $y_*$, $z_*$), $p_*$ is pressure, $\rho_*$ is density, $\bar{\rho}_*$ is the reference density, $t_*$ is time, and the differential operator $\nabla_* = (\partial/\partial x_*)\vec{i} + (\partial/\partial y_*)\vec{j} + (\partial/\partial z_*)\vec{k}$, where $\vec{i}$, $\vec{j}$ and $\vec{k}$ represent the unit vector in $x_*$, $y_*$ and $z_*$ directions.

The equations (1)-(3) can be made dimensionless as follows,

$$\nabla \cdot \mathbf{u} = 0, \tag{4}$$

$$\bar{\rho}\frac{\partial \mathbf{u}}{\partial t} + \bar{\rho}\mathbf{u} \cdot \nabla \mathbf{u} = -\nabla p - \frac{(\rho - \bar{\rho})}{Fr^2}\vec{k}, \tag{5}$$

$$\frac{\partial \rho}{\partial t} + \mathbf{u} \cdot \nabla \rho = 0, \tag{6}$$

where the dimensional quantities are made dimensionless using their respective characteristic scales, *i.e.*,

$$\left.\begin{aligned} \mathbf{x} = \frac{\mathbf{x}_*}{L}, \quad t = \frac{t_* V_c}{L}, \quad \mathbf{u} = \frac{\mathbf{u}_*}{V_c}, \\ p = \frac{p_*}{\Delta\rho_* V_c^2}, \quad \rho = \frac{\rho_*}{\Delta\rho_*}, \quad \bar{\rho} = \frac{\bar{\rho}_*}{\Delta\rho_*}, \end{aligned}\right\} \tag{7}$$

in which $\mathbf{x}$ is the dimensionless coordinate vector $(x\vec{i}+y\vec{j}+z\vec{k})$, $L$ is the characteristic length scale which is the thickness of the effective sheared layer determined by the streamwise velocity profile of the basic flow, $V_c$ and $\Delta\rho_*$ are the characteristic velocity and density scales which are the initial streamwise velocity and density changes across the sheared/stratified layer, respectively. $Fr = V_c/\sqrt{gL}$ in (5) is the *Froude* number.

It is assumed that the flow quantities consist of the basic flow and infinitesimal perturbations,

$$\mathbf{u}(\mathbf{x},t) = \mathbf{U}(z) + \mathbf{u}'(\mathbf{x},t), \tag{8}$$

$$\rho(\mathbf{x},t) = \rho_b(z) + \rho'(\mathbf{x},t), \tag{9}$$

$$p(\mathbf{x},t) = P(z) + p'(\mathbf{x},t) = p_0 - \frac{1}{Fr^2}\int_0^z \rho_b(z)dz + p'(\mathbf{x},t), \tag{10}$$

where $\mathbf{U}$ is the dimensionless basic flow velocity vector where the components in $x$, $y$ and $z$ directions are $U$, $V$ and $W$, $\rho_b$ is the dimensionless basic density profile, $p_0$ is the dimensionless reference pressure corresponding to the dimensionless reference density $\overline{\rho}$. The superscript symbol '$'$' represents the perturbation part of the corresponding physical property.

Both the basic flow and the total flow (basic flow + infinitesimal perturbations) are governed by the equations (4)-(6). By substituting (8)-(10) into (4)-(6) and assuming the product of an infinitesimal quantity and its gradient is negligible [4], *i.e.*, $\mathbf{u}'\cdot\nabla\mathbf{u}' \approx 0$ and $\mathbf{u}'\cdot\nabla\rho' \approx 0$, as well as noting that $\mathbf{U}\cdot\nabla\rho_b(z) = 0$, the following perturbation equations are deduced,

$$\nabla\cdot\mathbf{u}' = 0, \tag{11}$$

$$\overline{\rho}\frac{\partial\mathbf{u}'}{\partial t} + \overline{\rho}(\mathbf{U}\cdot\nabla\mathbf{u}' + \mathbf{u}'\cdot\nabla\mathbf{U}) = -\nabla p' - \frac{\rho'}{Fr^2}\vec{k}, \tag{12}$$

$$\frac{\partial\rho'}{\partial t} + \mathbf{U}\cdot\nabla\rho' + \mathbf{u}'\cdot\nabla\rho_b(z) = 0. \tag{13}$$

For the CSS flows considered here, all the basic flow properties are assumed to vary with the vertical coordinate $z$ only. In particular, the following basic flow velocities are assumed,

$$\mathbf{U}(z) = U(z)\vec{i} + V(z)\vec{j}.$$

The following normal mode is used in the subsequent linear stability analysis,

$$\phi'(\mathbf{x},t) = \hat{\phi}(z)e^{i(\alpha x+\beta y)-i\alpha ct} = \hat{\phi}(z)e^{i(\alpha x+\beta y)-\sigma t}, \tag{14}$$

where $i$ is the imaginary unit of a complex number, $\alpha$ and $\beta$ are the streamwise and spanwise wavenumbers, respectively, and the perturbation quantity $\phi'$ represents velocity, density, temperature, buoyancy flux, and other physical quantities. The hat symbol denotes the peak amplitude of the corresponding perturbation. $\sigma = -i\alpha c$ is the temporal growth rate of the perturbation, where $c$ is the wave (phase) speed.

Substituting the normal modes into (11)-(13) leads to,

$$i\alpha\hat{u} + i\beta\hat{v} + D\hat{w} = 0, \tag{15}$$

$$\overline{\rho}(\sigma + i\alpha U + i\beta V)\hat{u} + \overline{\rho}U_z\hat{w} = -i\alpha\hat{p}, \tag{16}$$

$$\overline{\rho}(\sigma + i\alpha U + i\beta V)\hat{v} + \overline{\rho}V_z\hat{w} = -i\beta\hat{p}, \tag{17}$$

$$\overline{\rho}(\sigma + i\alpha U + i\beta V)\hat{w} = -D\hat{p} - \frac{\hat{\rho}}{Fr^2}, \tag{18}$$

$$(\sigma + i\alpha U + i\beta V)\hat{\rho} + \rho_{b,z}\hat{w} = 0, \tag{19}$$

where $D = \partial/\partial z$ is the differential operator for the perturbation properties, and $\rho_{b,z} = \partial\rho_b(z)/\partial z$.

By applying the following Squire transformations [4],

$$\left.\begin{aligned} \tilde{\alpha} = (\alpha^2+\beta^2)^{1/2}, \quad \tilde{u} = \frac{\alpha\hat{u}+\beta\hat{v}}{\tilde{\alpha}}, \\ \tilde{p} = \frac{\tilde{\alpha}}{\alpha}\hat{p}, \quad \tilde{\rho} = \frac{\tilde{\alpha}}{\alpha}\hat{\rho}, \quad \tilde{b} = \frac{\tilde{\rho}}{\overline{\rho}}, \end{aligned}\right\} \tag{20}$$

where the hat symbols denote the Squire transformation properties, the three-dimensional perturbation equations (15)-(19) can be reduced, after a series of operations which are omitted here due to the page limit, to the following equivalent two-dimensional perturbation equations,

$$\tilde{\sigma}\begin{bmatrix} \nabla_s^2 & \\ & I \end{bmatrix}\begin{bmatrix} \hat{w} \\ \tilde{b} \end{bmatrix} = \begin{bmatrix} R_{11} & R_{12} \\ R_{21} & R_{22} \end{bmatrix}\begin{bmatrix} \hat{w} \\ \tilde{b} \end{bmatrix}, \tag{21}$$

where

$$\left.\begin{aligned} R_{11} = -i\tilde{\alpha}(U\nabla_s^2 - U_{zz}) - i\tilde{\alpha}\frac{\beta}{\alpha}\xi(\nabla_s^2 U - U_{zz}), \\ R_{12} = \frac{\tilde{\alpha}^2}{Fr^2}, \quad R_{21} = \tilde{N}^2, \quad R_{22} = -i\tilde{\alpha}U\left(1+\frac{\beta}{\xi}\right), \end{aligned}\right\} \tag{22}$$

where $\tilde{\sigma} = \sigma(\tilde{\alpha}/\alpha)$ is the Squire temporal growth rate of the perturbations properties and $\tilde{N}^2 = -\tilde{\rho}_{b,z}/\overline{\rho}$ is the local Squire buoyancy Brunt-Väisälä frequency. The Squire Laplacian operator $\nabla_s^2$ is defined as $\nabla_s^2 = D^2 - \tilde{\alpha}^2$. $\xi = V/U$ is the shear stress ratio and it is assumed that $U$ and $V$ have the same hyperbolic profile $f(z)$ but differing only in their amplitudes. If $\xi = 0$ or $\beta = 0$, (21) will reduce to the Taylor-Goldstein equation.

For inviscid sheared stratified flow, the velocity shear and the buoyancy form a single governing parameter, the local Richardson number $Ri_g(z_*)$, which is defined as,

$$Ri_g(z_*) = \frac{-(\partial b_*/\partial z_*)}{(\partial u_*/\partial z_*)^2} = \frac{N_*^2}{(\partial u_*/\partial z_*)^2} \tag{23}$$

where, again, the subscript '*' denotes the dimensional quantities, $b_* = g\rho_*/\overline{\rho}_*$ is the dimensional buoyancy, $N_*^2 = -g(\partial\rho_*/\partial z_*)/\overline{\rho}_*$ is the dimensional local Brunt-Väisälä frequency, and $\overline{\rho}_*$ is the dimensional reference density, respectively. Hazel [1] suggested that when the dimensionless basic velocity and background stratification are of the forms $\Delta u_0 f(z)$ and $\Delta\rho_0 f(z)$, where $\Delta u_0$ and $\Delta\rho_0$ are the velocity and density changes across the interficial layer and $f(z)$ is a hyperbolic function, and if $(\partial u/\partial z)|_{z=0} = 1$ and $(\partial\rho/\partial z)|_{z=0} = 1$, where $z = 0$ is the central line of the sheared/stratified layer, then $Ri_g(z)$ is determined by,

$$Ri_g(z) = \frac{N_*^2(z)}{(\partial u_*/\partial z_*)^2} = J\frac{-(\partial\rho/\partial z)}{(\partial u/\partial z)^2}. \tag{24}$$

in which $J = gL/(\overline{\rho}V_c^2) = 1/(\overline{\rho}Fr^2)$ is a dimensionless number, which has the same form as the bulk Richardson number of the flow and was introduced and used by Hazel [1] for PSS flows. As a result, $J$ will replace $Ri_g$ to become the dominant parameter for the CSS flows.

#### Methodology

The temporal mode of (21), where the wavenumbers $\alpha$ and $\beta$ are fixed as real numbers and $c$ is fixed as a complex number, is solved in this study in order to compare with the temporal mode analysis results on PSS flows by Hazel [1]. The matrix methods are used to solve the eigenvalue problems formed by

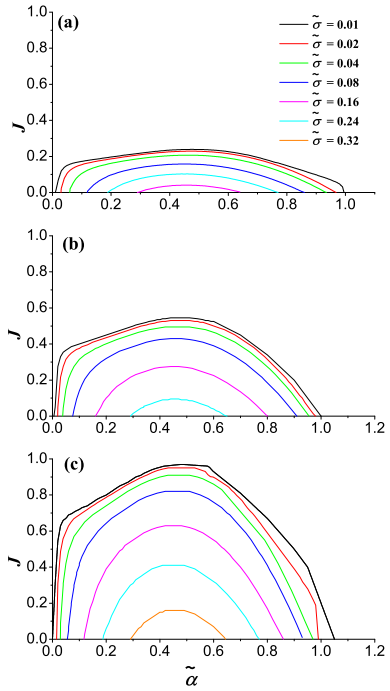


Figure 1. Contours of $\tilde{\sigma}$ in the $J-\tilde{\alpha}$ plane for the cross free sheared flows with (*a*) $\xi = 0$; (*b*) $\xi = 0.5$; and (*c*) $\xi = 1.0$, respectively.

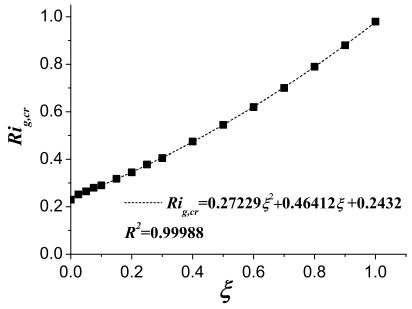


Figure 2. $Ri_{g,cr}$ plotted against $\xi$ for the cross free shear flows at $\tilde{\alpha} = 0.5$. The dash curve denote the parabolic correlation curve.

discretising (21) with uniform grids and using the second-order central difference scheme. The QZ algorithm integrated in the LAPACK routine CGGEV is used as the complex eigenvalue solver. The characteristic length scale $L$ is selected as one half of the sheared layer thickness and the maximum velocity in the computational domain is chosen as the characteristic velocity scale $V_c$. For all three types of CSS flows studied, the boundary conditions $u = w = v = b = 0$ are applied at both the top and bottom boundaries. $z$ varies between -5 and 5, same as that used by Hazel [1].

## Results

### Cross Free Sheared Flow

For cross free shear flows, the following typical hyperbolic functions are selected as the basic flow profiles,

$$U = tanh(z), \quad V = \xi tanh(z), \quad N^2 = J\,sech^2(z), \qquad (25)$$

where $U, V, N^2$ and $\xi$ are all dimensionless properties following the definitions of the previous section.

The stability analysis results for cross free sheared flows obtained by solving (21) with the matrix methods are presented in figure 1 where the contours of $\tilde{\sigma}$ are plotted in the $J-\tilde{\alpha}$ plane for the cross free shear flows with $\xi$ =0, 0.5 and 1.0, respectively. As the stability boundary with $\tilde{\sigma} = 0$ requires the matrix methods to use prohibitively large node numbers to obtain accurate solutions and the contour curve for $\tilde{\sigma} = 0.01$ is found to be almost the same as that for $\tilde{\sigma} = 0$ for PSS flows, the $\tilde{\sigma} = 0.01$ contour curve is thus approximated as the stability boundary for the unstable mode region. For the pure PSS flow case with $\xi = 0$ as shown in figure 1(*a*), the stability boundary follows exactly the same shape as that obtained by Hazel [1] with shooting methods. The critical local Richardson number $Ri_{g,cr}$, which corresponds to the location for the maximum $\tilde{\sigma}$ in the $J-\tilde{\alpha}$ plane, is close to, but less than, 0.25, the classic Miles-Howard theorem value. It is noted that all the solutions of $\tilde{\sigma}$ involve only the real part, indicating that the instability mode corresponds to the stationary wave mode where the instability will not propagate and detach the basic mean flow. In PSS flows, such a stationary wave mode corresponds to the Kelvin-Helmholtz instability. Similarly, only stationary solutions are obtained for all CSS flow cases considered. Nevertheless, it is interesting to note that all $\tilde{\sigma}$ contour curves with $\xi = 0.5$ and $\xi = 1.0$ stretch towards positive $J$ compared to those with $\xi = 0$. The extent of stretching is dependent on $\xi$, with the contour curves at $\xi = 1.0$ covering a larger region than the $\xi = 0.5$ case. A similar stretching behavior is also found for CSS flows with other $\xi$ values in the range $0 \le \xi \le 1$. Such a stretching effect increases notably the magnitude of $\tilde{\sigma}$ near the core of the stability curves, *e.g.*when $\xi$ is increased from 0 to 0.5 and to 1.0, $\tilde{\sigma}$ at the center increases from about 0.24 to 0.28 and to 0.32, respectively. More importantly, the increasing $\xi$ expands $Ri_{g,cr}$ to be far beyond the classic value of 0.25. For example, when $\xi = 0.5$, $Ri_{g,cr} = 0.53$; but if $\xi$ is increased to 1.0, $Ri_{g,cr}$ will increase to approximately 1.0 as well.

In order to quantify the dependence on $\xi$ of such a stretching effect, figure 2 presents the calculated $Ri_{g,cr}$ plotted against $\xi$ over $0 \le \xi \le 1.0$ for $\tilde{\alpha} = 0.5$, which demonstrates that the correlation between $Ri_{g,cr}$ and $\xi$ is a parabolic one. In some experimental studies and three-dimensional numerical simulations, occasional violations of the Miles-Howard theorem have been observed. It is noted that $Ri_{g,cr} = 0.25$ in figure 2 corresponds to $\xi \approx 0.1$ and when $\xi$ is increased beyond 0.1, $Ri_{g,cr}$ will be further increased to be higher than the classic value of 0.25. Hence, it is highly possible that these violations of the classic $Ri_{g,cr} = 0.25$ value are caused by the inevitable local cross shear in the three-dimensional instability.

### Cross Bounded Sheared Flow

On the basis of the free shear profiles (25), the cross bounded shear flows have the following profiles,

$$U = sin(z), \quad V = \xi sin(z), \quad N^2 = J. \qquad (26)$$

These profiles include the modifications from the solid boundary and are of the same forms as to those used by Hazel [1].

The obtained stability analysis results for cross bounded sheared flows are presented in figure 3. Compared to the cross free shear flows, the peak of $\tilde{\sigma}$, whose location corresponds to $Ri_{g,cr}$, moves towards the largest $\tilde{\alpha}$, at $\tilde{\alpha} \approx 0.8$. Similarly, as shown in figure 4 for $\tilde{\alpha} = 0.8$, $Ri_{g,cr}$ increases with $\xi$, again in a parabolic fashion.

### Cross Free Jet Flow

The basic cross jet flows have the following profiles,

$$U = sech(z), \quad V = \xi sech(z), \quad N^2 = J. \qquad (27)$$

The profiles for $U$ and $N$ are in the same forms as that used in [4] which are also similar to those used by Hazel [1]. The obtained

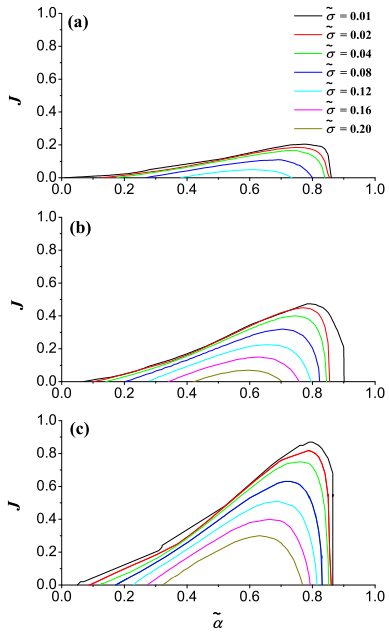


Figure 3. Contours of $\tilde{\sigma}$ in the $J-\tilde{\alpha}$ plane for the cross bounded sheared flows with (*a*) $\xi = 0$; (*b*) $\xi = 0.5$; and (*c*) $\xi = 1.0$, respectively.

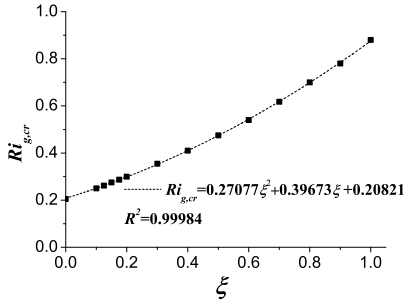


Figure 4. $Ri_{g,cr}$ versus $\xi$ for the cross bounded sheared flow at $\tilde{\alpha} = 0.8$.

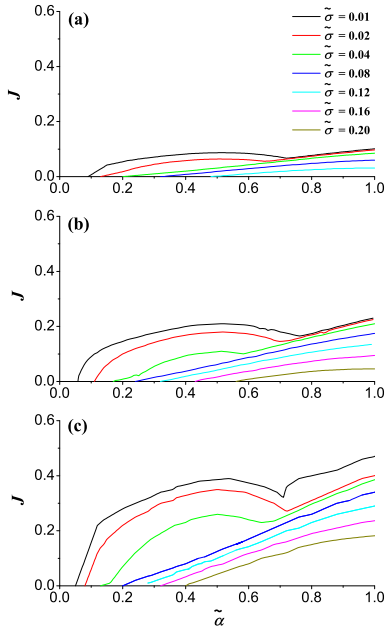


Figure 5. Contour plot of $\tilde{\sigma}$ at (a) $\xi = 0$, (b) $\xi = 0.5$ and (c) $\xi = 1.0$ for the cross jet flow.

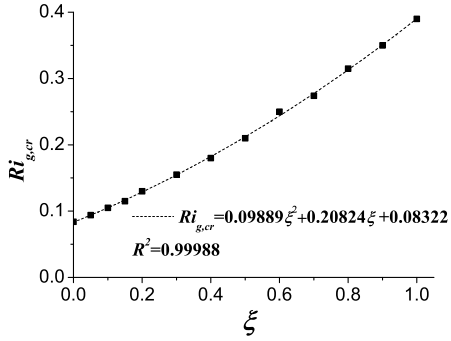


Figure 6. $Ri_{g,cr}$ versus $\xi$ for the cross free jet flow at $\tilde{\alpha} = 0.5$.

stability analysis results for cross free jet flows are presented in figure 5. For each $\tilde{\sigma}$ value, there are two peaks, and this study only examines the peak corresponding to the 'varicose mode' at a smaller wavenumber. The readers are referred to [4] for more information about the stability features of jet flows. A similar stretching effect observed for the other two types of CSS flows is also observed for the cross free jet flows. And again, as shown in figure 6 for $\tilde{\alpha} = 0.5$, $Ri_{g,cr}$ for the varicose mode increases with $\xi$, also in a parabolic fashion.

## Conclusions

With the introduction of the shear stress ratio $\xi$, linear perturbation equations are derived for CSS flows to obtain their stability features with comparable streamwise and spanwise velocities in the basic flow states. With the derived perturbation equations, the stability features of a cross free sheared flow, a cross bounded sheared flow, and a cross jet flow with specific velocity and stratification profiles are obtained. It is found that the unstable regions of all these three types of CSS flows stretch towards large values of the local Richardson number $Ri_g$ with the introduction of the spanwise velocity, and the growth rate of the perturbation increases significantly when $\xi$ increases. As a result of such a stretching effect, the stability boundary in terms of the critical local Richardson number $Ri_{g,cr}$ expands with increasing $\xi$ and exceeds the classic Miles-Howard theorem value of $Ri_{g,cr} = 0.25$.

## Acknowledgements

The support from the Australian Research Council (ARC), the National Natural Science Foundation of China (51469035, 11072211), and the Yunnan Natural Science Foundation (2011FA017) is gratefully acknowledged. Y. X. also thanks James Cook University for the JCUPRS scholarship.

## References

[1] Hazel, P., Numerical Studies of the Stability of Inviscid Stratified Shear Flows, *J. Fluid Mech.*, **51**, 1972, 39–61.

[2] Atsavapranee, P. and Gharib, M., Structures in Stratified Plane Mixing Layers and the Effects of Cross-Shear, *J. Fluid Mech.*, **342**, 1997, 53–86.

[3] Lin, J., Shao, X. and Yu, Z., Numerical Research on Coherent Structures in a Mixing Layer with Cross-Shear, *Acta Aeronautica et Astronautica Sinica*, **20**, 2000, 13–20.

[4] Drazin, P.G. and Reid, W.H., *Hydrodynamic Stability* (second edition), Cambridge University Press, 2004.